LETTER TO THE EDITOR

Transverse-momentum p_t correlations on (η, ϕ) from mean-p_t fluctuations in Au–Au collisions at $\sqrt{s_{NN}} = 200$ GeV

STAR Collaboration

J Adams[1], M M Aggarwal[2], Z Ahammed[3], J Amonett[4], B D Anderson[4], D Arkhipin[5], G S Averichev[6], S K Badyal[7], Y Bai[8], J Balewski[9], O Barannikova[10], L S Barnby[1], J Baudot[11], S Bekele[12], V V Belaga[6], A Bellingeri-Laurikainen[13], R Bellwied[14], J Berger[15], B I Bezverkhny[16], S Bharadwaj[17], A Bhasin[7], A K Bhati[2], V S Bhatia[2], H Bichsel[18], J Bielcik[16], J Bielcikova[16], A Billmeier[14], L C Bland[19], C O Blyth[1], S-L Blyth[20], B E Bonner[21], M Botje[8], A Boucham[13], J Bouchet[13], A V Brandin[22], A Bravar[19], M Bystersky[23], R V Cadman[24], X Z Cai[25], H Caines[16], M Calderón de la Barca Sánchez[9], J Castillo[20], O Catu[16], D Cebra[26], Z Chajecki[12], P Chaloupka[23], S Chattopadhyay[3], H F Chen[27], J H Chen[25], Y Chen[28], J Cheng[29], M Cherney[30], A Chikanian[16], H A Choi[31], W Christie[19], J P Coffin[11], T M Cormier[14], M R Cosentino[32], J G Cramer[18], H J Crawford[33], D Das[3], S Das[3], M Daugherity[34], M M de Moura[32], T G Dedovich[6], M DePhillips[19], A A Derevschikov[35], L Didenko[19], T Dietel[15], S M Dogra[7], W J Dong[28], X Dong[27], J E Draper[26], F Du[16], A K Dubey[36], V B Dunin[6], J C Dunlop[19], M R Dutta Mazumdar[3], V Eckardt[37], W R Edwards[20], L G Efimov[6], V Emelianov[22], J Engelage[33], G Eppley[21], B Erazmus[13], M Estienne[13], P Fachini[19], J Faivre[11], R Fatemi[38], J Fedorisin[6], K Filimonov[20], P Filip[23], E Finch[16], V Fine[19], Y Fisyak[19], K S F Fornazier[32], J Fu[29], C A Gagliardi[39], L Gaillard[1], J Gans[16], M S Ganti[3], F Geurts[21], V Ghazikhanian[28], P Ghosh[3], J E Gonzalez[28], H Gos[40], O Grachov[14], O Grebenyuk[8], D Grosnick[41], S M Guertin[28], Y Guo[14], A Gupta[7], N Gupta[7], T D Gutierrez[26], T J Hallman[19], A Hamed[14], D Hardtke[20], J W Harris[16], M Heinz[42], T W Henry[39], S Hepplemann[43], B Hippolyte[11], A Hirsch[10], E Hjort[20], G W Hoffmann[34], M J Horner[20], H Z Huang[28], S L Huang[27], E W Hughes[44], T J Humanic[12], G Igo[28], A Ishihara[34], P Jacobs[20], W W Jacobs[9], M Jedynak[40], H Jiang[28], P G Jones[1], E G Judd[33], S Kabana[42], K Kang[29], M Kaplan[45], D Keane[4], A Kechechyan[6], V Yu Khodyrev[35], B C Kim[31], J Kiryluk[38], A Kisiel[40], E M Kislov[6], J Klay[20], S R Klein[20], D D Koetke[41], T Kollegger[15], M Kopytine[4], L Kotchenda[22], K L Kowalik[20], M Kramer[46], P Kravtsov[22], V I Kravtsov[35], K Krueger[24], C Kuhn[11], A I Kulikov[6], A Kumar[2], R Kh Kutuev[5], A A Kuznetsov[6], M A C Lamont[16], J M Landgraf[19], S Lange[15], F Laue[19], J Lauret[19], A Lebedev[19], R Lednicky[6], C-H Lee[31], S Lehocka[6], M J LeVine[19], C Li[27], Q Li[14], Y Li[29], G Lin[16],

S J Lindenbaum[46], M A Lisa[12], F Liu[47], H Liu[27], J Liu[21], L Liu[47],
Q J Liu[18], Z Liu[47], T Ljubicic[19], W J Llope[21], H Long[28], R S Longacre[19],
M Lopez-Noriega[12], W A Love[19], Y Lu[47], T Ludlam[19], D Lynn[19],
G L Ma[25], J G Ma[28], Y G Ma[25], D Magestro[12], S Mahajan[7],
D P Mahapatra[36], R Majka[16], L K Mangotra[7], R Manweiler[41],
S Margetis[4], C Markert[4], L Martin[13], J N Marx[20], H S Matis[20],
Yu A Matulenko[35], C J McClain[24], T S McShane[30], F Meissner[20],
Yu Melnick[35], A Meschanin[35], M L Miller[38], N G Minaev[35], C Mironov[4],
A Mischke[8], D K Mishra[36], J Mitchell[21], B Mohanty[3], L Molnar[10],
C F Moore[34], D A Morozov[35], M G Munhoz[32], B K Nandi[3], S K Nayak[7],
T K Nayak[3], J M Nelson[1], P K Netrakanti[3], V A Nikitin[5], L V Nogach[35],
S B Nurushev[35], G Odyniec[20], A Ogawa[19], V Okorokov[22], M Oldenburg[20],
D Olson[20], S K Pal[3], Y Panebratsev[6], S Y Panitkin[19], A I Pavlinov[14],
T Pawlak[40], T Peitzmann[8], V Perevoztchikov[19], C Perkins[33], W Peryt[40],
V A Petrov[14], S C Phatak[36], R Picha[26], M Planinic[48], J Pluta[40], N Porile[10],
J Porter[18], A M Poskanzer[20], M Potekhin[19], E Potrebenikova[6],
B V K S Potukuchi[7], D Prindle[18], C Pruneau[14], J Putschke[20],
G Rakness[43], R Raniwala[17], S Raniwala[17], O Ravel[13], R L Ray[34],
S V Razin[6], D Reichhold[10], J G Reid[18], J Reinnarth[13], G Renault[13],
F Retiere[20], A Ridiger[22], H G Ritter[20], J B Roberts[21], O V Rogachevskiy[6],
J L Romero[26], A Rose[20], C Roy[13], L Ruan[27], M J Russcher[8], R Sahoo[36],
I Sakrejda[20], S Salur[16], J Sandweiss[16], M Sarsour[39], I Savin[5], P S Sazhin[6],
J Schambach[34], R P Scharenberg[10], N Schmitz[37], K Schweda[20], J Seger[30],
I Selyuzhenkov[14], P Seyboth[37], E Shahaliev[6], M Shao[27], W Shao[44],
M Sharma[2], W Q Shen[25], K E Shestermanov[35], S S Shimanskiy[6],
E Sichtermann[20], F Simon[38], R N Singaraju[3], N Smirnov[16], R Snellings[8],
G Sood[41], P Sorensen[20], J Sowinski[9], J Speltz[11], H M Spinka[24],
B Srivastava[10], A Stadnik[6], T D S Stanislaus[41], R Stock[15], A Stolpovsky[14],
M Strikhanov[22], B Stringfellow[10], A A P Suaide[32], E Sugarbaker[12],
M Sumbera[23], B Surrow[38], M Swanger[30], T J M Symons[20],
A Szanto de Toledo[32], A Tai[28], J Takahashi[32], A H Tang[8], T Tarnowsky[10],
D Thein[28], J H Thomas[20], A R Timmins[1], S Timoshenko[22], M Tokarev[6],
T A Trainor[18], S Trentalange[28], R E Tribble[39], O D Tsai[28], J Ulery[10],
T Ullrich[19], D G Underwood[24], G Van Buren[19], N van der Kolk[8],
M van Leeuwen[20], A M Vander Molen[49], R Varma[50], I M Vasilevski[5],
A N Vasiliev[35], R Vernet[11], S E Vigdor[9], Y P Viyogi[3], S Vokal[6],
S A Voloshin[14], W T Waggoner[30], F Wang[10], G Wang[4], G Wang[44],
X L Wang[27], Y Wang[34], Y Wang[29], Z M Wang[27], H Ward[34], J W Watson[4],
J C Webb[9], G D Westfall[49], A Wetzler[20], C Whitten Jr[28], H Wieman[20],
S W Wissink[9], R Witt[42], J Wood[28], J Wu[27], N Xu[20], Z Xu[19], Z Z Xu[27],
E Yamamoto[20], P Yepes[21], I-K Yoo[31], V I Yurevich[6], I Zborovsky[23],
H Zhang[19], W M Zhang[4], Y Zhang[27], Z P Zhang[27], C Zhong[25],
R Zoulkarneev[5], Y Zoulkarneeva[5], A N Zubarev[6] and J X Zuo[25]

[1] University of Birmingham, Birmingham, UK
[2] Panjab University, Chandigarh 160 014, India
[3] Variable Energy Cyclotron Centre, Kolkata 700 064, India
[4] Kent State University, Kent, OH 44242, USA
[5] Particle Physics Laboratory (JINR), Dubna, Russia
[6] Laboratory for High Energy (JINR), Dubna, Russia

[7] University of Jammu, Jammu 180 001, India
[8] NIKHEF and Utrecht University, Amsterdam, The Netherlands
[9] Indiana University, Bloomington, IN 47408, USA
[10] Purdue University, West Lafayette, IN 47907, USA
[11] Institut de Recherches Subatomiques, Strasbourg, France
[12] Ohio State University, Columbus, OH 43210, USA
[13] SUBATECH, Nantes, France
[14] Wayne State University, Detroit, MI 48201, USA
[15] University of Frankfurt, Frankfurt, Germany
[16] Yale University, New Haven, CT 06520, USA
[17] University of Rajasthan, Jaipur 302004, India
[18] University of Washington, Seattle, WA 98195, USA
[19] Brookhaven National Laboratory, Upton, NY 11973, USA
[20] Lawrence Berkeley National Laboratory, Berkeley, CA 94720, USA
[21] Rice University, Houston, TX 77251, USA
[22] Moscow Engineering Physics Institute, Moscow, Russia
[23] Nuclear Physics Institute AS CR, 250 68 Řež/Prague, Czech Republic
[24] Argonne National Laboratory, Argonne, IL 60439, USA
[25] Shanghai Institute of Applied Physics, Shanghai 201800, People's Republic of China
[26] University of California, Davis, CA 95616, USA
[27] University of Science and Technology of China, Anhui 230027, People's Republic of China
[28] University of California, Los Angeles, CA 90095, USA
[29] Tsinghua University, Beijing 100084, People's Republic of China
[30] Creighton University, Omaha, NE 68178, USA
[31] Pusan National University, Pusan, South Korea
[32] Universidade de Sao Paulo, Sao Paulo, Brazil
[33] University of California, Berkeley, CA 94720, USA
[34] University of Texas, Austin, TX 78712, USA
[35] Institute of High Energy Physics, Protvino, Russia
[36] Institute of Physics, Bhubaneswar 751 005, India
[37] Max-Planck-Institut für Physik, Munich, Germany
[38] Massachusetts Institute of Technology, Cambridge, MA 02139-4307, USA
[39] Texas A&M University, College Station, TX 77843, USA
[40] Warsaw University of Technology, Warsaw, Poland
[41] Valparaiso University, Valparaiso, IN 46383, USA
[42] University of Bern, 3012 Bern, Switzerland
[43] Pennsylvania State University, University Park, PA 16802, USA
[44] California Institute of Technology, Pasadena, CA 91125, USA
[45] Carnegie Mellon University, Pittsburgh, PA 15213, USA
[46] City College of New York, New York, NY 10031, USA
[47] Institute of Particle Physics, CCNU (HZNU), Wuhan 430079, People's Republic of China
[48] University of Zagreb, Zagreb HR-10002, Croatia
[49] Michigan State University, East Lansing, MI 48824, USA
[50] Indian Institute of Technology, Mumbai, India

Abstract

We present first measurements of the pseudorapidity and azimuth (η, ϕ) bin-size dependence of event-wise mean transverse-momentum $\langle p_t \rangle$ fluctuations for Au–Au collisions at $\sqrt{s_{NN}} = 200$ GeV. We invert that dependence to obtain p_t autocorrelations on differences $(\eta_\Delta, \phi_\Delta)$ interpreted to represent velocity/temperature distributions on (η, ϕ). The general form of the autocorrelations suggests that the basic correlation mechanism is parton fragmentation. The autocorrelations vary rapidly with collision centrality, which suggests that fragmentation is strongly modified by a dissipative

medium in the more central Au–Au collisions relative to peripheral or p–p collisions.

(Some figures in this article are in colour only in the electronic version)

Central Au–Au collisions at the Relativistic Heavy Ion Collider (RHIC) may generate a colour-deconfined medium (quark–gluon plasma or QGP) [1]. Some theoretical descriptions predict abundant low-p_t gluon production in the early stages of high-energy nuclear collisions, with rapid parton thermalization as the source of that medium [2–4]. Particle yields, spectra and high-p_t correlations from Au–Au collisions at $\sqrt{s_{NN}} = 130$ and 200 GeV provide tantalizing evidence that a coloured medium is produced [5–8]. Nonstatistical fluctuations of event-wise mean p_t $\langle p_t \rangle$ [9, 10] should help in determining the properties of that medium. A recent measurement of excess $\langle p_t \rangle$ fluctuations in Au–Au collisions at 130 GeV [10] revealed a large excess of fluctuations compared to independent-particle p_t production. The measurement was obtained at a single *scale* (bin size)—the STAR detector acceptance on (η, ϕ) for that analysis. Excess $\langle p_t \rangle$ fluctuations studied with Monte Carlo simulations have been attributed to low-p_t parton fragments (minijets) [11]. Measurements of $\langle p_t \rangle$ fluctuations could help in illuminating the role of minijets in nuclear collisions.

In this letter, we report the first measurements of the scale dependence of $\langle p_t \rangle$ fluctuations. Moreover, by inversion of the scale-dependent $\langle p_t \rangle$ variance distribution we obtain p_t *autocorrelations*, projections of two-particle distributions on momentum *difference variables* $(\eta_\Delta, \phi_\Delta)$, where e.g. $\eta_\Delta \equiv \eta_1 - \eta_2$ [12]. We compare the resulting p_t correlation patterns to known azimuthal correlations (e.g., elliptic flow) and jet angular correlations. We consider the possibility that minijets, as local *velocity correlations*, provide a dominating contribution to p_t correlations and quantify centrality dependencies which may describe *in-medium modification* of jet correlations. This analysis is based on $\sqrt{s_{NN}} = 200$ GeV Au–Au collisions observed with the STAR detector at the Relativistic Heavy Ion Collider (RHIC).

In each heavy ion collision, and within some region on (η, ϕ) called a *bin*, a number of individual particle p_ts are sampled from *local* p_t spectra. Local spectrum properties may deviate from the event-averaged p_t spectrum differently at each point on (η, ϕ) and differently in each event [13]. The bin-size (scale) dependence of *excess* event-wise $\langle p_t \rangle$ fluctuations measured by *variance difference* $\Delta\sigma^2_{p_t:n}(\delta\eta, \delta\phi)$ reflects the correlation structure of the local p_t spectrum properties [14]. Certain aspects of the correlation structure can be accessed when that scale dependence is inverted to obtain p_t autocorrelations [12]: those aspects which depend on relative separation of pairs of points but not on absolute position on (η, ϕ). The p_t autocorrelations for Au–Au collisions over a range of centralities, their structure and interpretation, are the main subjects of this paper. The next three paragraphs define the $\langle p_t \rangle$ fluctuation measure and outline the derivation of the integral equation which connects its scale variation to the corresponding autocorrelation distribution. These paragraphs may be omitted in a first reading.

In this analysis, the detector acceptance is divided into *macro*bins with scales $(\delta\eta, \delta\phi)$. Each macrobin (scales represented by δx for brevity) contains in each event some integrated particle multiplicity $n(\delta x)$ and total $p_t(\delta x)$ (scalar sum over particles in the bin). Rather than fluctuations of *ratio* $\langle p_t \rangle \equiv p_t/n$ (a source of systematic error), we study fluctuations of *difference* $(p_t - n\hat{p}_t)/\sqrt{\bar{n}}$. The scale-dependent *per-particle* p_t variance is defined by $\sigma^2_{p_t:n}(\delta x) \equiv \overline{(p_t(\delta x) - n(\delta x)\hat{p}_t)^2}/\bar{n}(\delta x)$, where $\hat{p}_t$ is the inclusive mean particle p_t, $\bar{n}$ is the mean bin multiplicity, $p_t{:}n$ reads p_t *given* multiplicity n and the overline represents an

average over all macrobins in all events [10]. The small-scale limit ($\bar{n} = 1$) of $\sigma^2_{p_t:n}(\delta x)$ is $\sigma^2_{\hat{p}_t}$, the inclusive single-particle variance. The *variance difference* is then defined as $\Delta\sigma^2_{p_t:n}(\delta x) \equiv \sigma^2_{p_t:n}(\delta x) - \sigma^2_{\hat{p}_t}$. Variation of $\Delta\sigma^2_{p_t:n}$ on scales $(\delta\eta, \delta\phi)$ corresponds to an integral equation which can be inverted to obtain p_t autocorrelations on difference variables $(\eta_\Delta, \phi_\Delta)$, which compactly represent two-particle p_t correlations on (η, ϕ) [15] and permit direct interpretation of $\langle p_t \rangle$ fluctuations in terms of physical mechanisms.

The autocorrelation distribution is a powerful tool for accessing two-particle correlations under certain conditions well satisfied in relativistic nuclear collisions [15]. An *auto*correlation compares a distribution $f(x)$ *to itself*. It is effectively a *projection by averaging* of product distribution $f(x_1) \cdot f(x_2)$ on (x_1, x_2) onto the difference variable $x_\Delta \equiv x_1 - x_2$. In this analysis, we obtain the autocorrelation of the p_t distribution on 2D space (η, ϕ). Autocorrelations can be determined by *pair counting* [15, 16] or by *inverting* fluctuation scale dependence to form density ratios following the procedure in [12] first implemented in [17]. Here we use the latter method.

We can relate variance measurements to autocorrelations in the following way. If a space x is partitioned into *micro*bins of fixed size ϵ_x, combined to form macrobins of variable size δx, the macrobin contents in $\sigma^2_{p_t:n}(\delta x)$ can be expressed as microbin sums, e.g., $p_t(\delta x) = \sum_a p_{t,a}(\epsilon_x)$, a being a microbin index. We can then express variance $\sigma^2_{p_t:n}(\delta x)$ as a double sum over microbin indices (a, b) on (x_1, x_2) of terms $\overline{(p_t - n\hat{p}_t)_a(p_t - n\hat{p}_t)_b}$, which measure the *covariance* between bins a and b on x of p_t fluctuations relative to $n\hat{p}_t$ [19]. As shown in [12, 17] we can rearrange the double sum into an outer sum over index k on difference variable $x_\Delta \equiv x_1 - x_2$ (e.g., $\eta_1 - \eta_2$, with microbin index k) and an inner sum over microbins on sum variable $x_1 + x_2$. The inner sum is p_t difference autocorrelation $\Delta A_k(p_t:n)$ ('difference' referring to $p_t - n\hat{p}_t$). If self-pairs are excluded from the microbin sums, the p_t difference autocorrelation corresponds to variance difference $\Delta\sigma^2_{p_t:n}(\delta x)$. We define reference *number* autocorrelation $A_{k,\text{ref}}(n)$ as the mean pair number $\bar{n}_k^2$ in the kth microbin on x_Δ obtained by averaging products of mean particle numbers $\bar{n}_a\bar{n}_b$ along the kth diagonal of (x_1, x_2), that is, with $a - b = k$. This reference is approximately equivalent to the mixed-pair reference autocorrelation which would be obtained by direct pair counting [12]. $A_{k,\text{ref}}(n)$ is not obtained explicitly in this analysis, is instead an implicit part of the density ratio defined below and inferred by fluctuation inversion. Autocorrelation *densities* $\rho(x_\Delta)$, defined e.g. by $\Delta A_k(p_t : n) \equiv \epsilon_x^2\Delta\rho(p_t : n; k\epsilon_x)$ and $A_{k,\text{ref}}(n) = \epsilon_x^2\rho_{\text{ref}}(n; k\epsilon_x)$, are independent of microbin size. The required per-particle autocorrelation measure corresponding to $\Delta\sigma^2_{p_t:n}(\delta x)$ is density ratio $\Delta\rho(p_t:n)/\sqrt{\rho_{\text{ref}}(n)} \equiv \Delta A(p_t:n)/\epsilon_x\sqrt{A_{\text{ref}}(n)}$ (units $(\text{GeV}/c)^2$), which estimates the p_t covariance per particle *for a given separation* on (η, ϕ), averaged over the acceptance[51]. Within an $O(1)$ constant factor, such density ratios have the form of Pearson's *correlation coefficient* [18]: the average covariance for all pairs of bins with a given separation on (η, ϕ) relative to the geometric mean of Poisson number variances for those bin pairs.

For this 2D scaling analysis, we generalize $\delta x \rightarrow (\delta\eta, \delta\phi)$ to obtain the per-particle conditional p_t variance difference (also defining difference factor $\Delta\sigma_{p_t:n}$ [10]) as the 2D discrete integral equation

$$\Delta\sigma^2_{p_t:n}(m_\delta\epsilon_\eta, n_\delta\epsilon_\phi) \equiv 2\sigma_{\hat{p}_t}\Delta\sigma_{p_t:n}(m_\delta\epsilon_\eta, n_\delta\epsilon_\phi)$$
$$= 4\sum_{k,l=1}^{m_\delta, n_\delta} \epsilon_\eta\epsilon_\phi K_{m_\delta n_\delta;kl} \frac{\Delta\rho(p_t : n; k\epsilon_\eta, l\epsilon_\phi)}{\sqrt{\rho_{\text{ref}}(n; k\epsilon_\eta, l\epsilon_\phi)}}, \tag{1}$$

[51] p_t correlation measure $\Delta\rho(p_t:n)/\sqrt{\rho_{\text{ref}}(n)}$ is related to the number-correlation measure in [15, 16] by $\bar{N}(\hat{r} - 1) \simeq 2\Delta\eta\Delta\phi\sqrt{\rho_{\text{ref}}}\Delta\rho/\rho_{\text{ref}} \simeq 24\Delta\rho(n)/\sqrt{\rho_{\text{ref}}(n)}$. It is also related to single-particle *conditional* distribution $1/N_{\text{trig}}\text{d}N/\text{d}\Delta\phi$ [6] but invokes no trigger condition.

with kernel $K_{m_\delta n_\delta;kl} \equiv (m_\delta - k + 1/2)/m_\delta \cdot (n_\delta - l + 1/2)/n_\delta$. This integral equation can be inverted to obtain autocorrelation density ratio $\Delta\rho/\sqrt{\rho_{\rm ref}}$ as a per-particle $p_{\rm t}$ correlation measure on $(\eta_\Delta, \phi_\Delta)$ from the scale dependence of $\langle p_{\rm t} \rangle$ fluctuations represented by variance difference $\Delta\sigma^2_{p_{\rm t}:n}(\delta\eta, \delta\phi)$ [12, 19].

Data for this analysis were obtained with the STAR detector [20] using a 0.5 T uniform magnetic field parallel to the beam axis. Event triggering and charged-particle measurements with the time projection chamber (TPC) are described in [20]. Track definitions, tracking efficiency and background corrections, event and track quality cuts and primary-particle definition are similar to those described in [10, 21] for 130 GeV. While there are quantitative differences between the two energies and detector configurations, the better quality of full-magnetic-field tracking at 200 GeV tends to more than offset the effect of larger track densities there compared to the half-field tracking at 130 GeV. The difference between backgrounds is a few per cent of the total track yield (larger for 200 GeV) and is included in the corrections. Tracks were accepted with pseudorapidity in the range $|\eta| < 1$, transverse momentum in the range $p_{\rm t} \in [0.15, 2]$ GeV/c and 2π azimuth, defining the detector acceptance for this analysis. Particles identification was not implemented. Eleven centrality classes were defined as fractions of $\sigma_{\rm tot}$ (nine equal fractions from 90% to 10%, the top 10% being further divided in half). The centralities specified below, rounded to the nearest 5%, are within 2% of the defined values. Centralities were determined using the uncorrected number N of charged particles in $|\eta| < 1$ [22].

Figure 1 (left panels) shows the scale dependence of variance difference $\Delta\sigma^2_{p_{\rm t}:n}(\delta\eta, \delta\phi)$ in equation (1) for 3 of the 11 centralities analysed. The scale axes are divided into microbins: 16 on pseudorapidity scale $\delta\eta$ and 24 on azimuth scale $\delta\phi$. Variance differences typically increase monotonically with $\delta\eta$ but have more complex behaviour on $\delta\phi$. Measurements of difference factor $\Delta\sigma_{p_{\rm t}:n}$ at $\sqrt{s_{\rm NN}} = 130$ GeV reported in [10] correspond to the single point at the STAR acceptance scale $(2, 2\pi)$ for each centrality. To access the underlying dynamics, we extract the corresponding autocorrelation distributions. Figure 1 (right panels) shows 2D autocorrelations (by construction symmetric about $\eta_\Delta, \phi_\Delta = 0$) inferred from fluctuation scale dependence in the left panels by inverting equation (1) [12]. Autocorrelations have distinct same-side ($|\phi_\Delta| < \pi/2$) and away-side ($|\phi_\Delta| > \pi/2$) components. For peripheral collisions (top-right panel), the same-side peak appears to be nearly symmetric on $(\eta_\Delta, \phi_\Delta)$, however, cf the peak widths in figure 3. In general, the correlation structure evolves rapidly with centrality.

Errors for $\langle p_{\rm t} \rangle$ fluctuation measurements in figure 1 (left panels) are discussed in [10]. Statistical errors for those variance differences are typically less than 0.001 (GeV/c)^2 for all scales and centralities. The inversion process (effectively a differentiation, which acts as a 'high-pass' filter) tends to exaggerate small-wavelength noise on the autocorrelation. Control of that noise during inversion requires a standard procedure called *regularization*, in which each bin of $\Delta\rho/\sqrt{\rho_{\rm ref}}$ is treated as a χ^2 fitting parameter, incorporating a smoothing term with corresponding Lagrange multiplier into the χ^2 expression [12, 17]. Autocorrelation errors then have two components: statistical noise which survives smoothing and systematic error due to image distortion by smoothing. Statistical errors on the autocorrelation are estimated by inverting the noise estimate for $\Delta\sigma^2_{p_{\rm t}:n}$. The per-bin *rms* statistical error which survives smoothing is about 0.0002 (GeV/c)^2 for all autocorrelations. The smoothing distortion, estimated by passing data through the inversion process twice and comparing the resulting two autocorrelation versions [12, 17], typically peaks at about 5% of the maximum autocorrelation value at points of maximum gradient. Correlation amplitudes inferred from model fits (see below) were corrected for tracking inefficiencies and background contamination [10]. An overall systematic error of ±14% for corrected amplitudes reflects uncertainty in extrapolation of variance-difference measurements to the true number of primary particles in the acceptance.
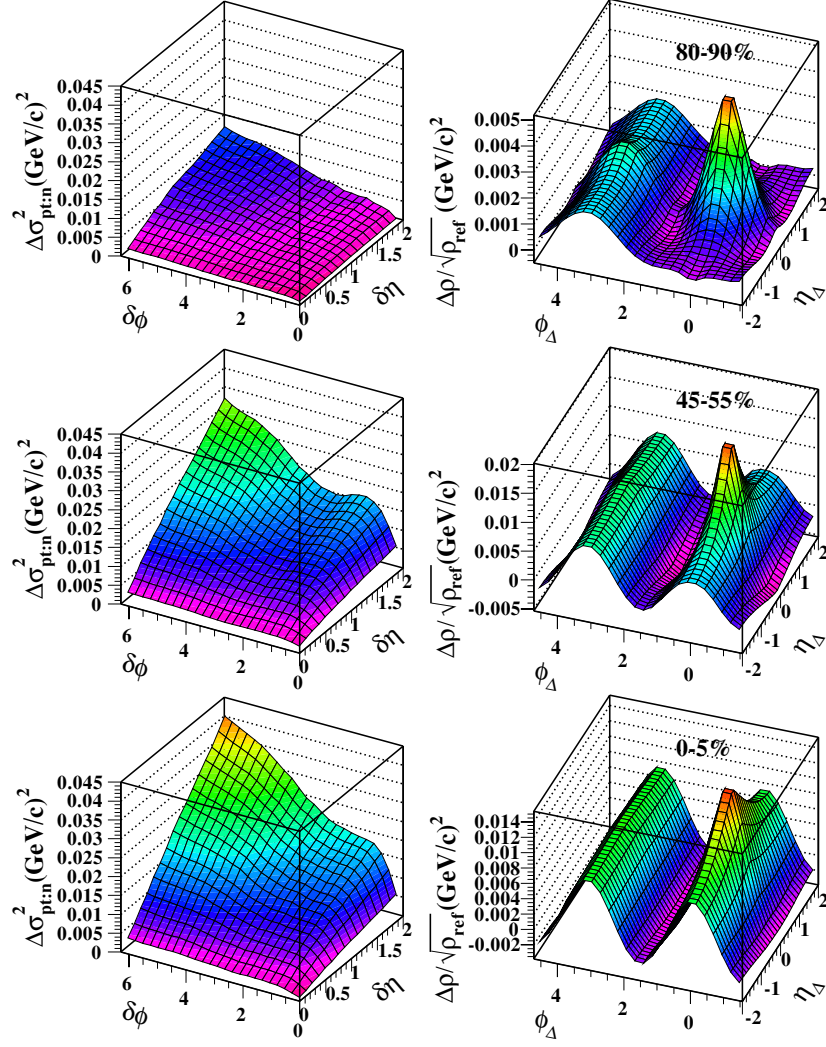
Figure 1. Left panels: $\Delta\sigma^2_{p_t:n}$ $(GeV/c)^2$ distributions on scale $(\delta\eta, \delta\phi)$ for three centrality bins: 80–90% of total cross section (top panel), 45–55% of total cross section (middle panel) and 0–5% of total cross section (bottom panel). Right panels: corresponding autocorrelations on difference variables $(\eta_\Delta, \phi_\Delta)$.

In figure 2, monopole (constant offset), dipole $\cos(\phi_\Delta)$ and quadrupole $\cos(2\phi_\Delta)$ components (sinusoids evident in figure 1, right panels) have been subtracted from the autocorrelations for centralities (80–90, 45–55, 20–30 and 0–5%) by minimizing residuals of the three components on the away side ($|\phi_\Delta| > \pi/2$) and for $|\eta_\Delta| \sim 2$ (minimizes influence of away-side peak structure). The full-ϕ-acceptance fluctuations in figure 1 (left panels) are determined only by the minijet structure and the monopole component; the dipole and quadrupole components integrate to zero at $\delta\phi = 2\pi$. Since one interpretation of p_t correlations is that they reflect velocity correlations of local particle source velocities, the quadrupole component from this analysis may constitute the first observation of elliptic flow as a *true velocity phenomenon*.
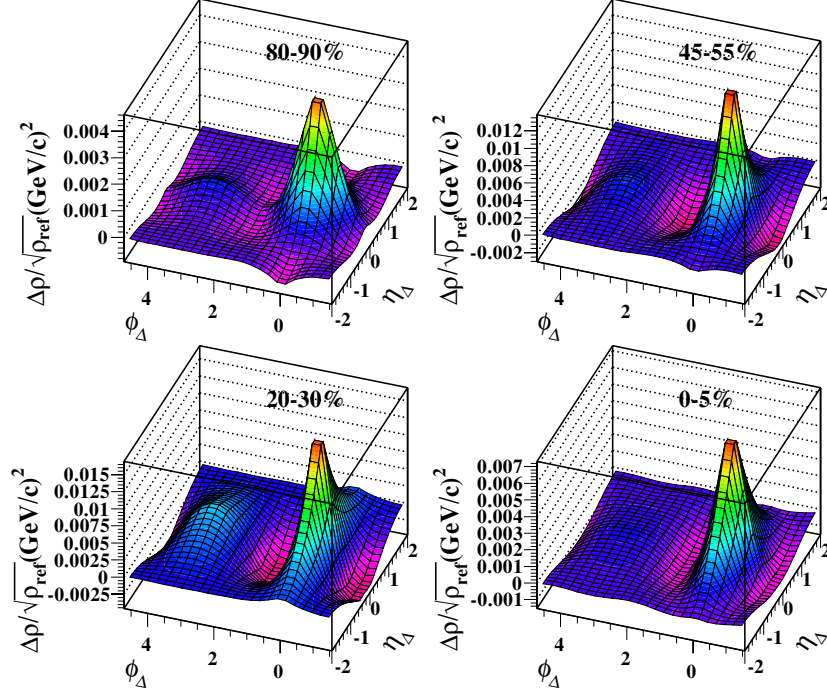
Figure 2. Distributions of $\Delta\rho/\sqrt{\rho_{\mathrm{ref}}}(\eta_\Delta, \phi_\Delta)$ for 80–90% (upper left), 45–55% (upper right), 20–30% (lower left) and 0–5% (lower right) of total cross section. Monopole (constant), dipole and quadrupole components have been subtracted.

The subtracted autocorrelations retain three structures localized on both η_Δ and ϕ_Δ: a same-side positive peak, a same-side negative peak (apparent as the regions of *negative* correlation immediately adjacent to the positive peak on ϕ_Δ) and an away-side peak. The near-side negative peak cannot be a result of incorrect subtraction of the multipole components. The latter have by definition no structure (are constant) on η_Δ, whereas the negative near-side peak is highly structured (a peak rising symmetrically to zero) on η_Δ. The near-side positive peak, in the absence of alternative explanations, is interpretable as a velocity correlation associated with semi-hard parton scattering (minijets). Those three p_t correlation structures comprise the main subject of this paper.

In figure 2, we observe that the three peak features vary strongly in shape and amplitude with collision centrality. For the more central collisions, we observe that the same-side positive peak is substantially elongated along η_Δ and significantly *narrowed* along ϕ_Δ. We quantify those observations with model fits. The autocorrelations in figure 2 were fitted with the model function defined in equation (2), a sum of near-side positive peak B_1, near-side negative peak B_2 (signed number) and away-side peak B_3, each with the same form,

$$F = \sum_{i=1}^{3} B_i \exp\left\{ -\left|\frac{\eta_\Delta}{\sqrt{2}\sigma_{\eta i}}\right|^{\tau_{\eta i}} - \left|\frac{\phi_\Delta - \delta_{i3}\pi}{\sqrt{2}\sigma_{\phi i}}\right|^{\tau_{\phi i}} \right\}, \tag{2}$$

where δ_{i3} is a Kronecker delta. This function includes exponents τ as shape parameters. In contrast to a Gaussian ($\tau \equiv 2$), which best describes near-side peaks for number autocorrelations [16], best-fit exponents for these p_t autocorrelations were found to be $\tau_{\eta 1} = \tau_{\eta 3} = \tau_{\phi 1} = 1.5 \pm 0.1$, with $\tau_{\phi 2} = 2.5 \pm 0.1$, $\tau_{\phi 3} = 1.9 \pm 0.1$ and $\tau_{\eta 2} = 1.7 \pm 0.1$ (for all centralities). Widths for near-side negative and away-side peaks varied (respectively, from
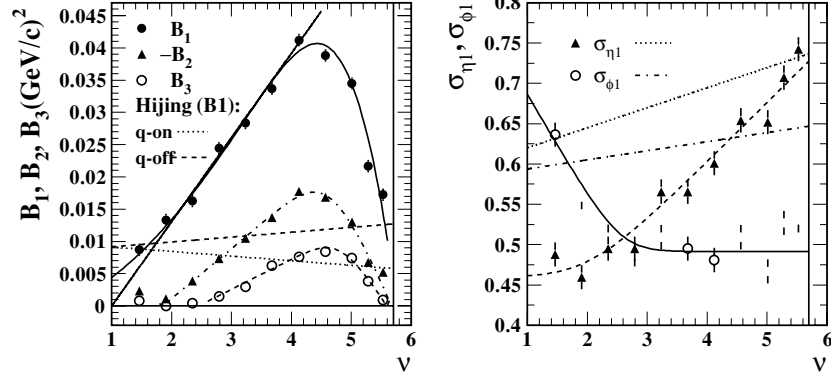
Figure 3. Correlation amplitudes (left panel) plotted versus mean participant path length ν. Solid dots are for positive near-side peaks and solid triangles are for negative near-side peaks. Open circles are for away-side peaks. Positive-peak widths (right panel) are plotted on ν for pseudorapidity (solid triangles) and azimuth (open circles). Curves guide the eye (see the text). Dotted, dashed and dash-dotted lines represent Hijing results.

peripheral to central) nearly linearly over the ranges $0.75 < \sigma_{\eta 2} < 1.1 \pm 0.1, 0.9 < \sigma_{\eta 3} < 1 \pm 0.1, \sigma_{\phi 2} \sim 2.1 \pm 0.2$ and $2.4 > \sigma_{\phi 3} > 1.5 \pm 0.1$.

The best-fit amplitudes for all peaks, corrected for background contamination and tracking inefficiency (21–38% for these 200 GeV data, increasing from minimum to maximum centrality) [10], and widths for the near-side positive peak are plotted in figure 3 versus mean participant path length ν.[52] The vertical line to the right of each panel indicates the estimated limit of ν for Au–Au collisions, corresponding to $b \sim 0$ and $N_{\text{part}}/2 \sim 191$. The fitted peaks are strongly localized on η_Δ and are very different in shape from the η_Δ-independent sinusoid components subtracted from autocorrelations in figure 1 (right panels) to form those in figure 2. There is therefore negligible cross-talk between the two types of fitting functions. The difference between fitting the data in figure 1 (right panels) including sinusoids in the model function and the data in figure 2 with equation (2) is less than the stated errors in the fit parameters. Residuals from fitted peak structures were typically less than 2% of the near-side peak amplitude. The peak amplitudes increase with centrality to a maximum value and then decrease sharply for the most central collisions. The near-side positive-peak width on η_Δ increases monotonically with centrality, while that on ϕ_Δ decreases. The rising part of the B_1 data is consistent with both a straight line $\propto (\nu - 1)$ and a curve $\propto \nu^{1.6}$.

The autocorrelation density ratio $\Delta\rho(p_t{:}n)/\sqrt{\rho_{\text{ref}}(n)}$ measures *relative covariances* (proportional to Pearson's correlation coefficient) of $\langle p_t \rangle$ fluctuations at pairs of points on (η, ϕ) separated by $(\eta_\Delta, \phi_\Delta)$. The autocorrelation distribution reveals the *average* shape of localized structures which may appear in different places on (η, ϕ) in different events, and possibly in only some events, but which have some shape stability over an event ensemble. We observe substantial (0.01–0.1) p_t covariances which can be interpreted as local transverse-velocity and/or temperature fluctuations correlated at pairs of points on (η, ϕ). As with the separation of temperature and transverse-flow aspects of inclusive single-particle p_t distributions, temperature and velocity correlations may also be distinguished as to source mechanism if mass identification is implemented in p_t fluctuation/correlation analysis.

The structures in figures 1 (right panel) and 2 can be compared to signature angular correlations for high-p_t parton fragments: a same-side 2D peak at the origin (jet cone) and an

---

[52] ν estimates the mean participant path length in number of encountered nucleons [22].

away-side η_Δ-invariant ridge on ϕ_Δ (apparent as such only in 2D analyses like this one). The correlations in figure 1 (upper-right panel) have exactly that structure and agree in detail with the Hijing correlations described below which are known to represent low-p_t jets, providing strong evidence that the dominant source of p_t correlations for p–p and peripheral Au–Au collisions is low-p_t parton fragments. For low-p_t partons, the away-side ridge in figure 1 (upper-right panel) is not distinguishable from one lobe of a sinusoid and is thus removed in the multipole subtraction to obtain figure 2. The same-side positive peak then represents the conventional jet-cone structure, albeit in p_t rather than angular correlations. We can then argue that the same features for more central Au–Au collisions continue to derive from low-p_t partons, but with modifications by a coloured dissipative medium.

The model-fit results in figure 3 illustrate the dramatic changes in figure 2 structure with collision centrality. Focusing on the near-side positive peak, the width on ϕ_Δ falls by 30%, whereas the width on η_Δ increases by 60%. Those trends are qualitatively similar to equivalent measurements of angular correlations [16], where the large width increase on η_Δ was interpreted as due to strong coupling of low-p_t partons to the longitudinally expanding coloured medium. The σ_η variation is much less for p_t correlations, suggesting that elongation of parton fragment distributions on η involves lower-p_t particles with increasing η_Δ. The near-side peak for p_t correlations is significantly non-Gaussian, the sharper peak represented by exponent $\tau = 1.5$ (the correspondent for angular correlations is a Gaussian with $\tau = 2$).

The amplitude B_1 of the near-side positive peak increases by a factor of 4 or more with centrality, but falls off rapidly for the most central collisions, in contrast to the subtracted monopole term which increases monotonically to mid centrality and then remains constant with further centrality increase. Since the relative covariance could also be interpreted (with strong assumptions) as a number of correlated pairs per particle in the system, the increase of B_1 may indicate that the number of correlated pairs from minijets increases *relative to the total multiplicity*. If the system were composed only of *independent* minijets (with no soft particle production), the autocorrelation density ratio (and variance difference) would be independent of system size (minijet number). The observed increase with system size could then result from a larger number of low-p_t partons, a larger mean fragment multiplicity for each parton, or both. The other correlation structures, the negative same-side and positive away-side peaks, are unique to p_t correlations and will be considered in detail in a follow-up publication. The presence of the negative near-side peak means that the variance difference, as an integral fluctuation measure, significantly underestimates the relative amount of minijet structure.

An equivalent analysis of $\langle p_t \rangle$ fluctuations in Hijing collisions [17] indicates that the near-side peak shapes for Hijing (quench on or quench off) are nearly symmetric on $(\eta_\Delta, \phi_\Delta)$, with shape described by single exponent $\tau = 1.7 \pm 0.1$. The combination of same-side 2D peak and away-side 1D azimuthal ridge observed in that analysis supports the interpretation that the basic source of those p_t correlations is low-p_t parton fragments or minijets, consistent with the basic pQCD jet model in Hijing. The centrality dependence of the amplitudes of the Hijing near-side peak for quench-on (default) and quench-off collisions is represented, respectively, by dotted and dashed lines in figure 3 (left panel). The lines in the right panel correspond to Hijing default (quench on) same-side peak widths. The amplitude (width) centrality trends for default Hijing are similar: modest variations linear with path length ν. The differences between quench-on and quench-off results from central Au–Au collisions for amplitudes and widths, representing pQCD modelling of in-medium parton energy loss, are $\sim 10\%$.

Comparing Hijing to the present analysis in figure 3, we note that there are at least three instances of qualitative disagreement between Hijing and RHIC data. First, for very peripheral Au–Au collisions (and therefore nucleon–nucleon collisions) the Hijing same-side

peak (jet cone) is symmetric on angle, whereas the data are quite asymmetric. Thus, there is already disagreement with data at the level of parton fragmentation in elementary collisions. Second, the centrality dependencies of the amplitudes and widths of the same-side peak are qualitatively different from data: in some cases even the sign of the variation is wrong. Third, the amplitude of the same-side Hijing peak is qualitatively less than that for data in mid-central collisions. The last is especially surprising when comparing quench-off Hijing (dashed line in the left panel) to data. The quench-off Hijing option in principle models jet production from a linear superposition of N–N collisions combined with a Glauber model of a *transparent* nucleus. That model should provide an upper limit for jet structure in A–A collisions. Yet the same-side peak amplitude for quench-off Hijing is 2–3 times *less* than that for mid-central RHIC Au–Au collisions which are observed to be *highly opaque* to minijets in the central region. Finally, we observe no evidence in Hijing data for the same-side negative peak which is a prominent new feature of RHIC data. The perturbative treatment of parton energy loss in Hijing appears to disagree strongly with the observed process for the minimum-bias partons which dominate p_t correlations in Au–Au collisions.

In conclusion, we have for the first time measured the scale dependence of $\langle p_t \rangle$ fluctuations on $(\delta\eta, \delta\phi)$ in heavy ion collisions. We have inverted those distributions to obtain autocorrelation distributions on corresponding difference variables $(\eta_\Delta, \phi_\Delta)$ which reveal the correlation structure of the local properties of a two-particle p_t distribution, specifically a combination of local transverse velocity and temperature. Inferred autocorrelations reveal complex p_t correlation structure in Au–Au collisions at RHIC, including peaked structures attributed to minijets which vary strongly with collision centrality. We observe that p_t autocorrelations provide unique access to minijet structure down to very low p_t and probe the detailed interplay between low-p_t partons and the dissipative coloured medium. Further studies with identified particles may separately characterize the local velocity and temperature structures of heavy ion collisions.

Acknowledgments

References

[1] Collins J C and Perry M J 1975 *Phys. Rev. Lett.* **34** 1353
Freedman B and McLerran L 1978 *Phys. Rev.* D **17** 1109
Baym G and Chin S A 1976 *Phys. Lett.* B **62** 241
Cabibbo N and Parisi G 1975 *Phys. Lett.* B **59** 67
Cabibbo N and Parisi G 2004 *Proc. Quark Matter 2004, J. Phys. G: Nucl. Part. Phys.* **30** S633
[2] Kajantie K, Landshoff P V and Lindfors J 1987 *Phys. Rev. Lett.* **59** 2527
[3] Mueller A H 2000 *Nucl. Phys.* B **572** 227
[4] Nayak G C, Dumitru A, McLerran L and Greiner W 2001 *Nucl. Phys.* A **687** 457
[5] d'Enterria D 2003 *Preprint* nucl-ex/0309015
[6] Adler C *et al* (STAR Collaboration) 2003 *Phys. Rev. Lett.* **90** 082302

[7]   Adler C *et al* (STAR Collaboration) 2002 *Phys. Rev. Lett.* **89** 202301
[8]   Adams J *et al* (STAR Collaboration) 2003 *Phys. Rev. Lett.* **91** 172302
[9]   Adcox K *et al* 2002 *Phys. Rev.* C **66** 024901
[10] Adams J *et al* (STAR Collaboration) 2005 *Phys. Rev.* C **71** 064906
[11] Liu Q J and Trainor T A 2003 *Phys. Lett.* B **567** 184
[12] Trainor T A, Porter R J and Prindle D J 2005 *J. Phys. G: Nucl. Part. Phys.* **31** 809
[13] Adams J *et al* (STAR Collaboration) 2004 *Preprint* nucl-ex/0408012
[14] Trainor T A 2000 *Preprint* hep-ph/0001148
[15] Adams J *et al* (STAR Collaboration) 2006 *Phys. Lett.* B **634** 347
[16] Adams J *et al* (STAR Collaboration) 2004 *Preprint* nucl-ex/0411003
[17] Liu Q J, Prindle D J and Trainor T A 2006 *Phys. Lett.* B **632** 197
[18] Kenney J F and Keeping E S 1962 *Mathematics of Statistics: Part 1* 3rd edn (Princeton, NJ: Van Nostrand-Reinhold)
[19] Prindle D J and Trainor T A (STAR Collaboration) 2005 *Proc. MIT Workshop on Correlations and Fluctuations in Relativistic Nuclear Collisions (Cambridge, MA, 21–23 April 2005) J. Phys.: Conf. Ser.* **27** 118
[20] Ackermann K H *et al* 2003 *Nucl. Instrum. Methods* A **499** 624; see other STAR papers in volume 499
[21] Adler C *et al* (STAR Collaboration) 2001 *Phys. Rev. Lett.* **87** 112303
      Adler C *et al* (STAR Collaboration) 2002 *Phys. Rev. Lett.* **89** 202301
[22] Trainor T A and Prindle D J 2004 *Preprint* hep-ph/0411217